Science Advances
AAAS

advances.sciencemag.org/cgi/content/full/5/5/eaav4119/DC1

Supplementary Materials for

Metal-organic framework based on hinged cube tessellation as transformable mechanical metamaterial

Eunji Jin, In Seong Lee, Dongwook Kim, Hosoowi Lee, Woo-Dong Jang, Myung Soo Lah, Seung Kyu Min*, Wonyoung Choe*

*Corresponding author. Email: skmin@unist.ac.kr (S.K.M.); choe@unist.ac.kr (W.C.)

Published 10 May 2019, *Sci. Adv.* **5**, eaav4119 (2019)
DOI: 10.1126/sciadv.aav4119

The PDF file includes:

Scheme S1. Synthetic procedure of 3-TCPP.
Fig. S1. Characterization of BPY as a pillar in UPF-1.
Fig. S2. Coordination environment of Zn^{2+} ion of new SBU, $[(Zn(COO)_3(\mu_2–O)Zn(COO)_3]$.
Fig. S3. Packing of rhombicuboctahedron and cuboid of UPF-1.
Fig. S4. Thermogravimetric analysis data for UPF-1.
Fig. S5. ^{1}H NMR data for trace of solvent content in the UPF-1.
Fig. S6. Simulated and experimental PXRD patterns of UPF-1 from 100 to 313 K.
Fig. S7. Perspective view of the (002) and (220) planes in UPF-1.
Fig. S8. Thermal expansion coefficients of UPF-1.
Fig. S9. Transformation of a cuboid in UPF-1.
Fig. S10. Schematic representation in a corotating model.
Fig. S11. Calculated θ values from temperature-dependent PXRD data of UPF-1.
Fig. S12. Schematic illustration of the corotating model.
Fig. S13. Calculated (x, y) coordinates from 0° to 90°, derived from equation.
Fig. S14. Energy as a function of deformations D_i's.
Table S1. Temperature-dependent cell parameters (Å) and unit cell volume (Å^3) data from synchrotron PXRD.
Table S2. Temperature-dependent SCXRD of UPF-1.
Table S3. Thermal expansion coefficients from the a and c parameters and cell volume of SCXRD.
Table S4. Thermal expansion coefficients from the a and c parameters and cell volume of PXRD.
Table S5. Thermal expansion coefficient of reported solid-state structures.
Table S6. The values of d_1, d_2 and volume of cuboid depending on temperature.
Table S7. Optimized lattice parameters L_y (L_y^*) and bond angles Zn─O─Zn projected on the xy plane with respect to strained L_x's.

Table S8. Stiffness tensor components (C_{ij}'s) of UPF-1 in GPa.
Table S9. Elastic constants of UPF-1.
Table S10. Poisson's ratio of a variety of materials.
Reference (*53*–*76*)

Other Supplementary Material for this manuscript includes the following:

(available at advances.sciencemag.org/cgi/content/full/5/5/eaav4119/DC1)

Data file S1 (.cif format). Crystallographic data for UPF-1_193K.
Data file S2 (.cif format). Crystallographic data for UPF-1_213K.
Data file S3 (.cif format). Crystallographic data for UPF-1_233K.
Data file S4 (.cif format). Crystallographic data for UPF-1_253K.
Data file S5 (.cif format). Crystallographic data for UPF-1_273K.
Data file S6 (.cif format). Crystallographic data for UPF-1_293K.
Data file S7 (.cif format). Crystallographic data for UPF-1_313K.
Data file S8 (.pdf format). checkCIF for crystal structures of UPF-1_193K.
Data file S9 (.pdf format). checkCIF for crystal structures of UPF-1_213K.
Data file S10 (.pdf format). checkCIF for crystal structures of UPF-1_233K.
Data file S11 (.pdf format). checkCIF for crystal structures of UPF-1_253K.
Data file S12 (.pdf format). checkCIF for crystal structures of UPF-1_273K.
Data file S13 (.pdf format). checkCIF for crystal structures of UPF-1_293K.
Data file S14 (.pdf format). checkCIF for crystal structures of UPF-1_313K.
Movie S1 (.avi format). Animation of hinged cube tessellation.
Movie S2 (.mp4 format). Rotating movement of UPF-1 structure depending on temperature.

Ligand Synthesis

5,10,15,20-tetrakis(3-carboxyphenyl)porphyrin (3-TCPP) was synthesized by modifying original synthetic procedure (*53*). Synthesis of the linker consists of two steps (Scheme S1).

Synthesis of 1. 0.425 mL of distilled pyrrole (6.12 mmol) and 1 g (6.09 mmol) of 3-carbomethoxybenzaldehyde was dissolved in 350 mL of dry CH_2Cl_2. Ar gas was purged in the solution for 30 min. After then, the solution was protected from light. The mixture added 0.2 mL of BF_3 etherate (1.62 mmol) via syringe reacted at room temperature for 1 h. 1.15 g of p-chloranil (4.67 mmol) added in the solution was reacted at room temperature for 24 h. After reaction had finished, solvent was removed using a rotary evaporator. The silica gel was added in solution of a small volume. After then, all solvent was removed in the mixture and the compound was dried in vacuum. Through the column, impurities were separated from product using $CHCl_3$. First yellow impurity was removed in column and the crude porphyrin could be separated with 2–4% acetone in $CHCl_3$. After then, the crude product was purified by recrystallization using methanol and $CHCl_3$ in low temperature. The product was obtained as a purple powder (0.28 g, 5.7 %). ^{1}H NMR ($CDCl_3$, 400 MHz, ppm) δ 8.89 (s, 4H), 8.80 (s, 8H), 8.49 (d, 4H), 8.40 (d, 4H), 3.99 (s, 12H), –2.792 (s, 2H).

Synthesis of 3-TCPP. The 0.25 g of **1** (0.295 mmol) was dissolved in 40 mL THF. 1.65 g of KOH (0.0295 mol) dissolved in 1 mL of H_2O was added in the solution. After then, the mixture was reacted for 24 h using reflux. THF was totally removed using rotary evaporator after reaction had finished. The crude product was protonated using 2N HCl solution (30 mL). The obtained precipitate had green color and was filtered, washed with water, and dried. The green powder was dissolved in 10 mL of pyridine for neutralization and the solvent was totally removed by rotary evaporator. The purple solid was washed with water, filtered and dried under a vacuum. The final product $C_{48}H_{30}O_8N_4 \cdot (C_{10}H_4N_2)_{1.7}$ was obtained as a purple powder. ^{1}H NMR (DMSO-d_6, 400 MHz, ppm) δ 13.25 (s, 4H), 8.82 (s, 8H), 8.70 (s, 4H), 8.55 (d, 2H), 8.48 (d, 4H), 8.41 (d, 4H), 7.96 (t, 4H), 7.76 (t, 1H), 7.35 (t, 2H), –2.792 (s, 2H).

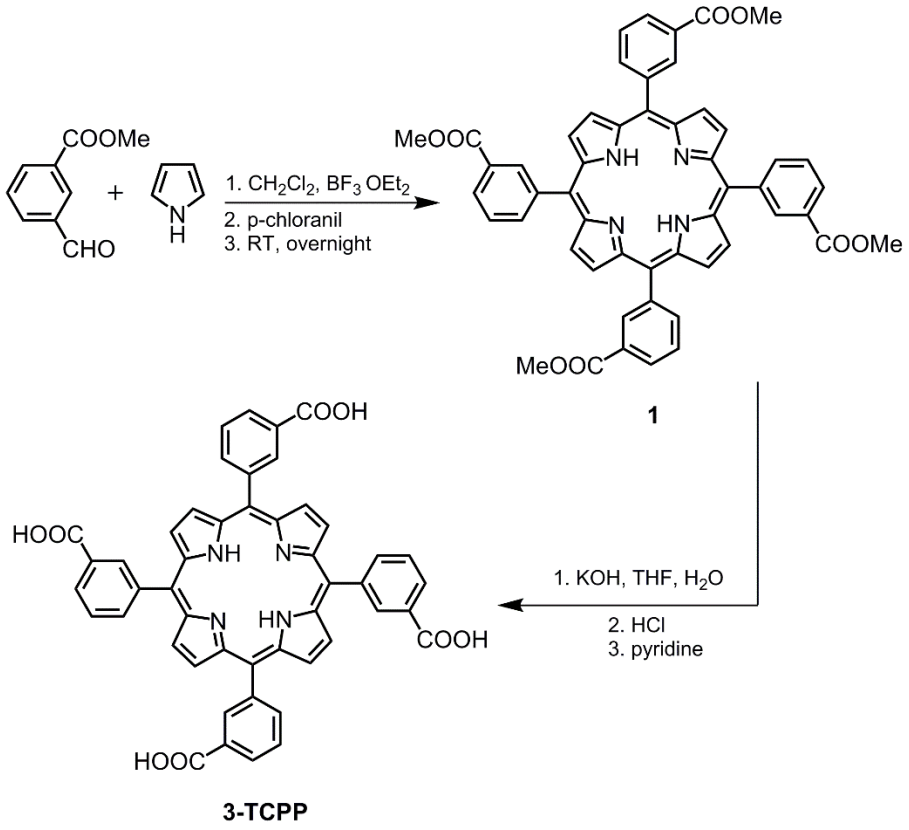

Scheme S1. Synthetic procedure of 3-TCPP.

Characterization of UPF-1

The amount of BPY in UPF-1 was confirmed by ^{1}H NMR spectrum after the acid digestion. Although the ratio of 3-TCPP linker and BPY from the crystal structure is 6 : 5, experimental ratio of two components was confirmed to be 6 : 3.6. The BPY in the structure was easily released in solution due to Zn–N distance. 832 compounds with Zn–BPY–Zn bonds found in Cambridge Structural Database (CSD).

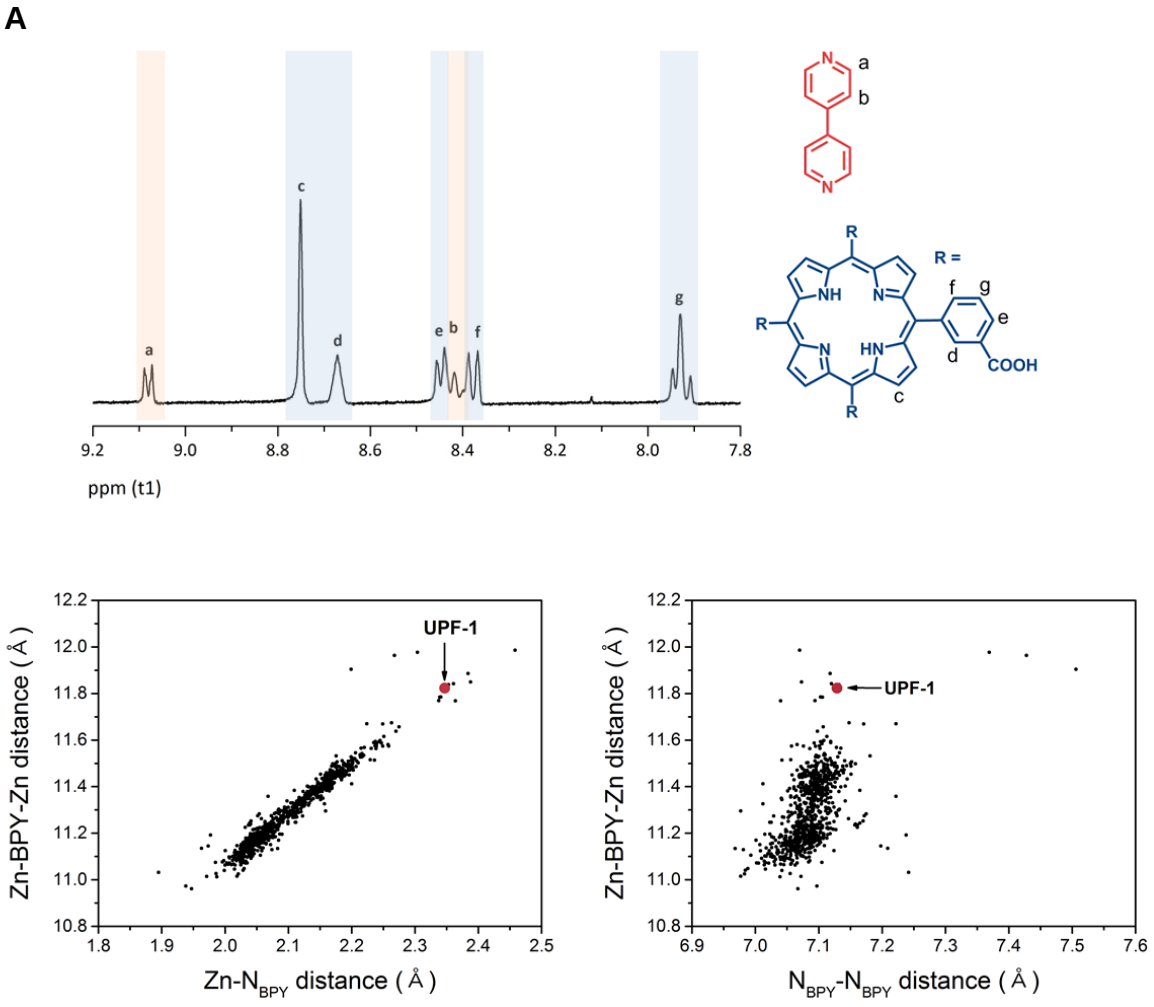

Fig. S1. Characterization of BPY as a pillar in UPF-1. (**A**) ^{1}H NMR spectrum of UPF-1 after acid digestion. The mother liquor (DMF/EtOH, v/v=3:1) was removed from the vial and the crystals were dried under vacuum overnight. The activated crystals were digested using 0.5 mL of DMSO-d_6 and 0.1 mL of dilute DCl (0.01 mL of 35 % DCl in D_2O in 0.5 mL of DMSO-d_6). Red and blue boxes represent signals of BPY and 3-TCPP linker, respectively. (**B**) Distance of Zn–N_{BPY} and Zn–BPY–Zn (left) and distance of N_{BPY}–N_{BPY} and Zn–BPY–Zn (right) found in CSD.

Structural analysis of UPF-1

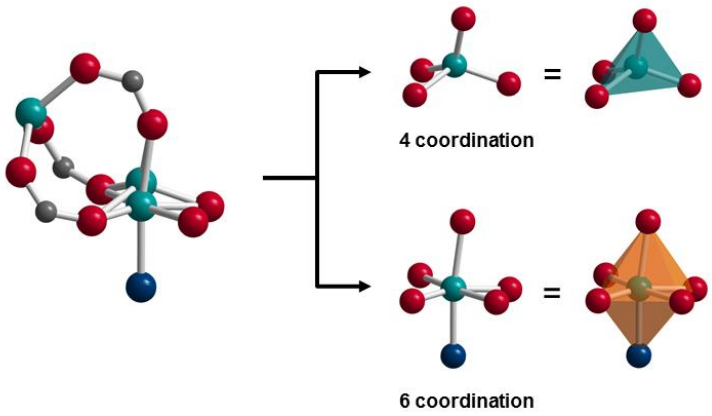

Fig. S2. Coordination environment of Zn^{2+} ion of new SBU, [$(Zn(COO)_3(\mu_2–O)Zn(COO)_3$]. The disordered Zn ion was represented by tetrahedral (dark green) and octahedral geometry (orange) as coordinated molecules. Zn, dark green; C, grey; O, red; N, blue.

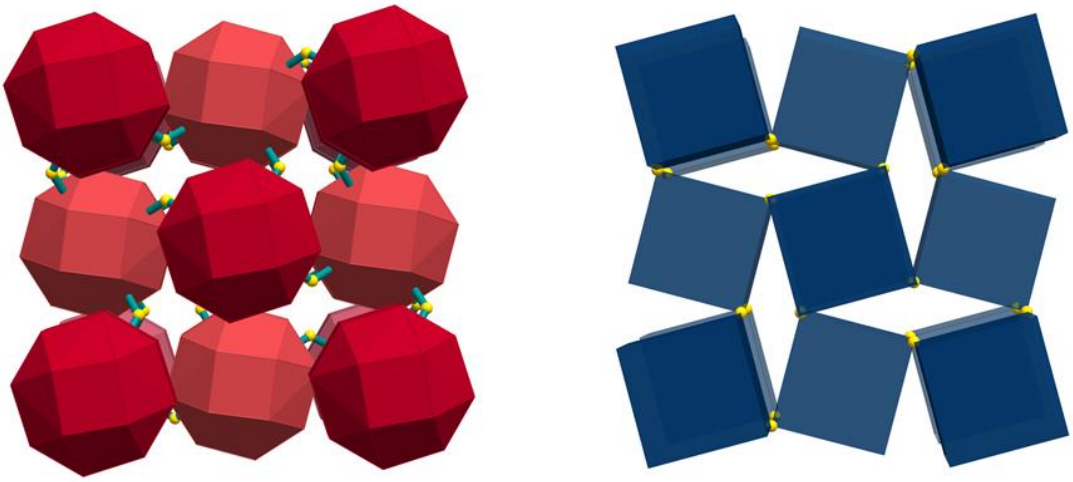

Fig. S3. Packing of rhombicuboctahedron and cuboid of UPF-1.

Thermogravimetric analysis of UPF-1

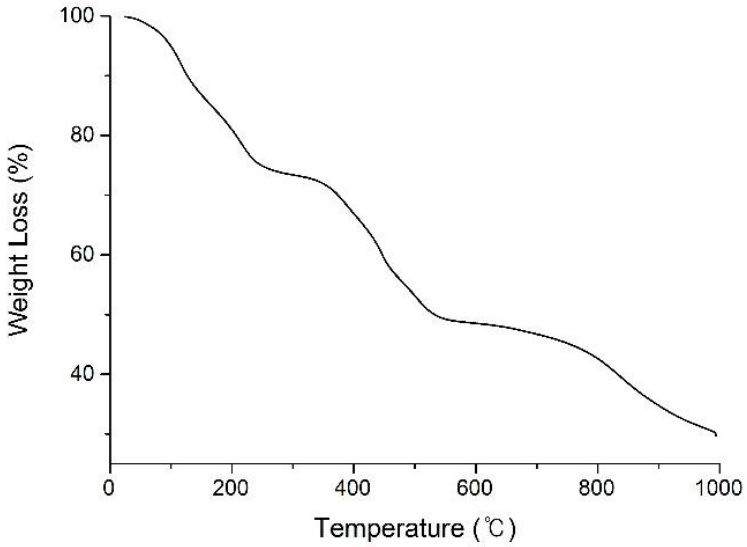

Fig. S4. Thermogravimetric analysis data for UPF-1. The initial weight loss (~75 %, 25–200 °C) represents removal of solvents. The next weight loss represents decomposition of structure around 380 °C (~50 %).

Solvent content of UPF-1

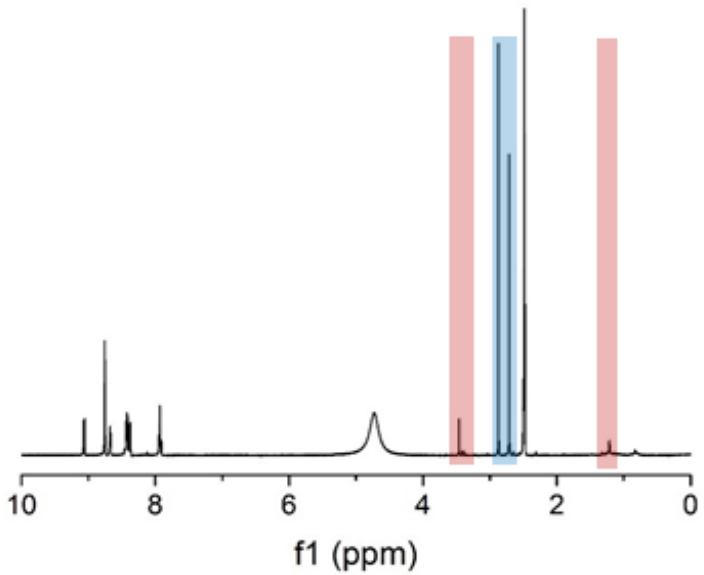

Fig. S5. ^{1}H NMR data for trace of solvent content in the UPF-1. The collected crystals were digested using 0.5 mL of DMSO-d_6 and 0.1 mL of dilute DCl (0.1 mL of 35 % DCl in D_2O in 0.5 mL DMSO-d_6). DMF and EtOH were included in the crystals at a ratio of 6:1.

Temperature-dependent synchrotron powder X-ray diffraction of UPF-1

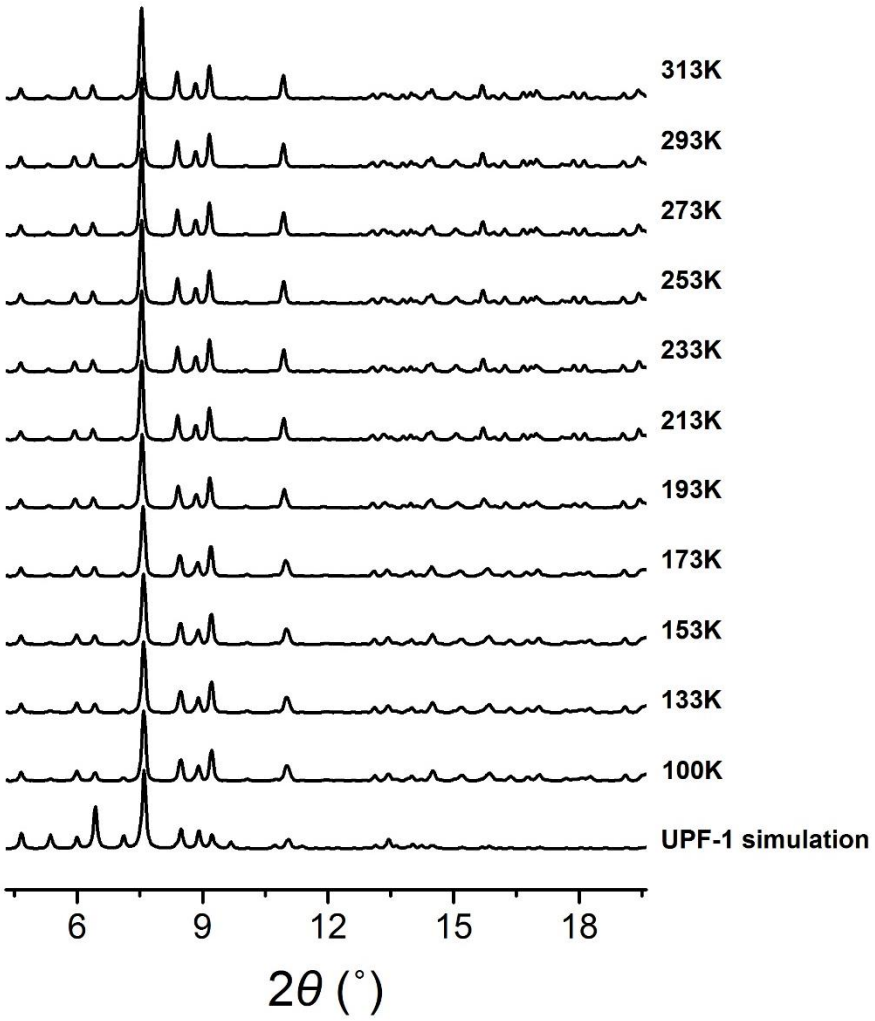

Fig. S6. Simulated and experimental PXRD patterns of UPF-1 from 100 to 313 K.

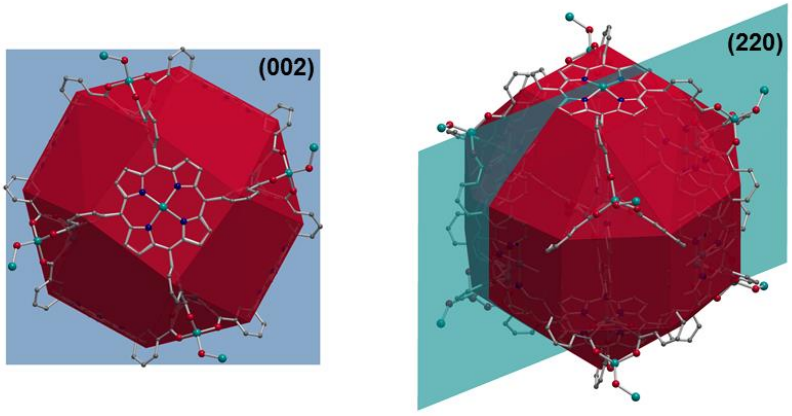

Fig. S7. Perspective view of the (002) and (220) planes in UPF-1.

Table S1. Temperature-dependent cell parameters (Å) and unit cell volume (Å^3) data from synchrotron PXRD.

T (K)	*a* (Å)	*c* (Å)	*V* (Å^3)
100	29.883(10)	34.403(8)	30722.59
133	29.880(16)	34.419(12)	30728.84
153	29.903(7)	34.424(10)	30780.39
173	29.942(4)	34.451(5)	30885.71
193	30.1444(8)	34.480(8)	31331.88
213	30.183(6)	34.484(10)	31415.65
233	30.188(8)	34.471(14)	31412.99
253	30.188(6)	34.482(11)	31424.74
273	30.207(7)	34.486(10)	31467.72
293	30.213(5)	34.476(8)	31470.84
313	30.237(5)	34.447(10)	31493.22

Temperature-dependent single-crystal X-ray diffraction of UPF-1

Table S2. Temperature-dependent SCXRD of UPF-1.

Formula	C_{158} $H_{83.20}$ $N_{14.80}$ $O_{35.80}$ Zn_{11}	C_{158} $H_{83.20}$ $N_{14.80}$ $O_{35.80}$ Zn_{11}	C_{158} $H_{83.20}$ $N_{14.80}$ $O_{35.80}$ Zn_{11}
T (K)	193(2)	213(2)	233(2)
Crystal system	tetragonal	tetragonal	tetragonal
Space group	*P4/mnc*	*P4/mnc*	*P4/mnc*
a (Å)	29.915(4)	30.221(4)	30.315(4)
c (Å)	34.378(7)	34.460(7)	34.474(7)
V (Å^3)	30765(11)	31473(11)	31682(11)
Z	4	4	4
R1 [I > 2σ(I)]	0.1291	0.1312	0.1200
wR2 [I > 2σ(I)]	0.4306	0.4297	0.4170
R1 [all data]	0.1380	0.1407	0.1291
wR2 [all data]	0.4435	0.4437	0.4320

Formula	C_{158} $H_{83.20}$ $N_{14.80}$ $O_{35.80}$ Zn_{11}	C_{158} $H_{83.20}$ $N_{14.80}$ $O_{35.80}$ Zn_{11}	C_{158} $H_{83.20}$ $N_{14.80}$ $O_{35.80}$ Zn_{11}
T (K)	253(2)	273(2)	293(2)
Crystal system	tetragonal	tetragonal	tetragonal
Space group	*P4/mnc*	*P4/mnc*	*P4/mnc*
a (Å)	30.326(4)	30.334(4)	30.344(4)
c (Å)	34.476(7)	34.473(7)	34.461(7)
V (Å^3)	31706(11)	31721(11)	31731(11)
Z	4	4	4
R1 [I > 2σ(I)]	0.1242	0.1145	0.1111
wR2 [I > 2σ(I)]	0.4204	0.3950	0.3808
R1 [all data]	0.1340	0.1273	0.1256
wR2 [all data]	0.4354	0.4122	0.3992

Formula	$C_{158}\ H_{83.20}\ N_{14.80}\ O_{35.80}\ Zn_{11}$
T (K)	313(2)
Crystal system	tetragonal
Space group	*P4/mnc*
a (Å)	30.373(4)
c (Å)	34.439(7)
V (Å^3)	31772(11)
Z	4
R1 [I > 2σ(I)]	0.1012
wR2 [I > 2σ(I)]	0.3521
R1 [all data]	0.1268
wR2 [all data]	0.3769

Thermal expansion coefficient (α)

A

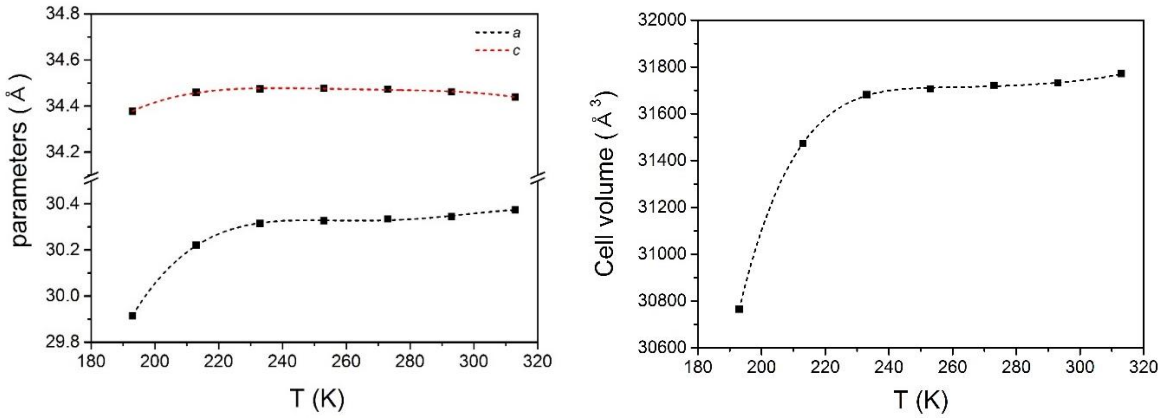

B

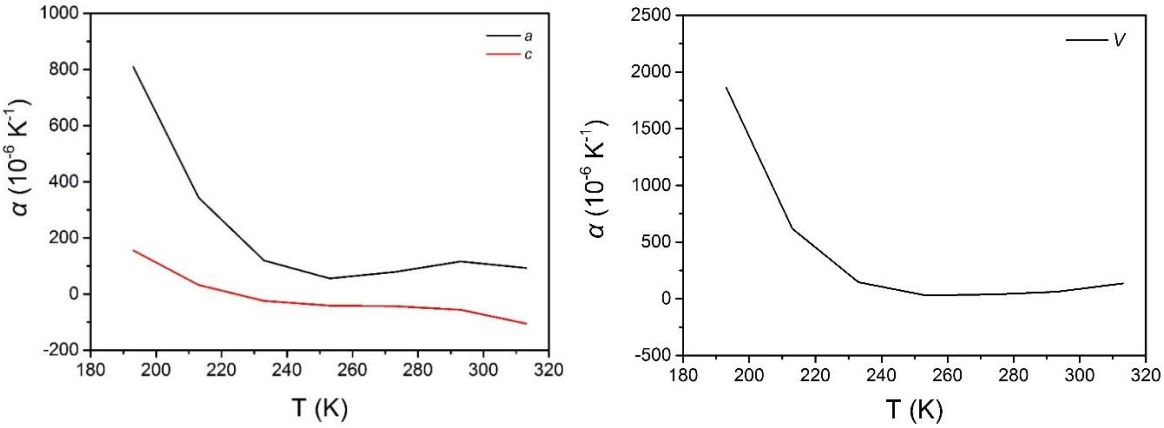

Fig. S8. Thermal expansion coefficients of UPF-1. (**A**) The fitting graph for thermal expansion coefficients of UPF-1 obtained from SCXRD data. (**B**) Temperature-dependent thermal expansion coefficient of *a* and *c* parameters, and cell volume.

Table S3. Thermal expansion coefficients from the *a* and *c* parameters and cell volume of SCXRD.

T (K)	α_a (10^{-6} K^{-1})	α_c (10^{-6} K^{-1})	α_V (10^{-6} K^{-1})
193	809.59	155.35	1862.95
213	343.67	32.32	618.21
233	119.23	–24.66	145.53
253	55.65	–41.44	32.04
273	78.80	–43.47	37.52
293	115.55	–56.23	60.79
313	92.83	–105.20	135.51
Average	230.76	–11.90	413.22

Table S4. Thermal expansion coefficients from the *a* and *c* parameters and cell volume of PXRD.

T (K)	α_a (10^{-6} K^{-1})	α_c (10^{-6} K^{-1})	α_V (10^{-6} K^{-1})
100	–3.80	13.78	6.16
133	38.39	7.06	83.88
153	65.98	38.93	171.08
173	338.07	43.13	722.29
193	64.07	5.57	133.68
213	7.42	–19.07	–4.23
233	1.36	16.00	18.70
253	31.32	5.70	68.39
273	9.82	–14.63	4.96
293	38.68	–41.78	35.56
313	-	-	-
Average	59.13	5.47	124.05

Table S5. Thermal expansion coefficient of reported solid-state structures.

Compound	T (K)	max α (10^{-6} K^{-1})				Ref
		a	***b***	***c***	***V***	
UPF-1	100−313	+338	-	+43	+722	This work
ZrW_2O_8	0.4−430	−9.1	-	-	-	*54*
$Ag_3[Co(CN)_6]$	20−297	+150	-	−130	-	*38*
FMOF-1	90−295	+230	-	−170	+300	*55*
(*S*,*S'*)-octa-3,5-diyn-2,7-diol	225−330	+515	−85	−204	+241	*56*
HMOF-1	160−320	+177	−21	-	-	*34*
Ag(mim)	20−300	+130	+44	−24.5	-	*57*
Cd(im)	100−300	+93	−23	+20	+120	*41*
MCF-18·DMF	119−295	-	-	+437	+353	*45*
MCF-34·DMF	233−299	+36	+237	−116	+157	*58*
[Zn(OH)niba]·MeOH	100−295	−41	−41	+166	+121	*35*
α PHA	223−348	+260	+39	−80	+248	*59*
$[Ag(en)]NO_3$-I	120−360	+149	−90	+38	+96	*60*
MCF-82	112−300	+61	+482	−218	+319	*61*
$\{[FeTp(CN)_3]_2]_2Co(Bib)_2\}_5\cdot H_2O$	180−240	+85	+278	+1089	+1498	*62*
fu-MOF (compound 1)	303−463	−380	+1161	+15	+837	*63*

Geometric model

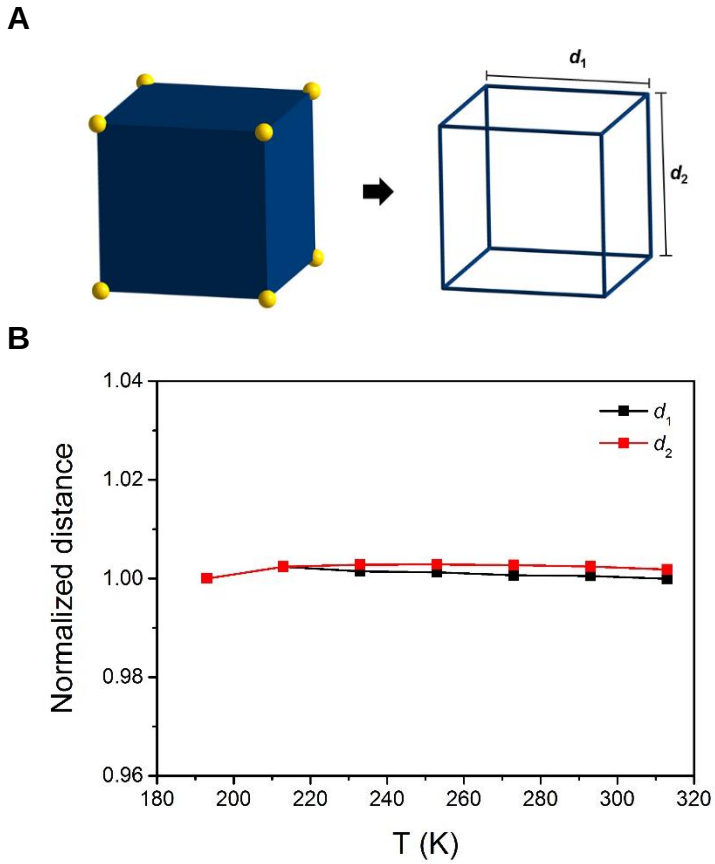

Fig. S9. Transformation of a cuboid in UPF-1. (**A**) Definition of d_1 and d_2 in cuboid (d_1: width, d_2: height). (**B**) Normalized distance of d_1 and d_2 depending on temperature.

Table S6. The values of d_1, d_2 and volume of cuboid depending on temperature.

T (K)	d_1 (Å)	d_2 (Å)	BOX V (Å^3)
193	17.31	17.19	5148.66
213	17.35	17.23	5185.42
233	17.33	17.24	5177.96
253	17.33	17.24	5176.47
273	17.32	17.24	5169.30
293	17.32	17.23	5166.61
313	17.31	17.22	5157.35
Average	17.32	17.23	5168.83

Calculation of θ and cartesian coordinates based on a co-rotating model

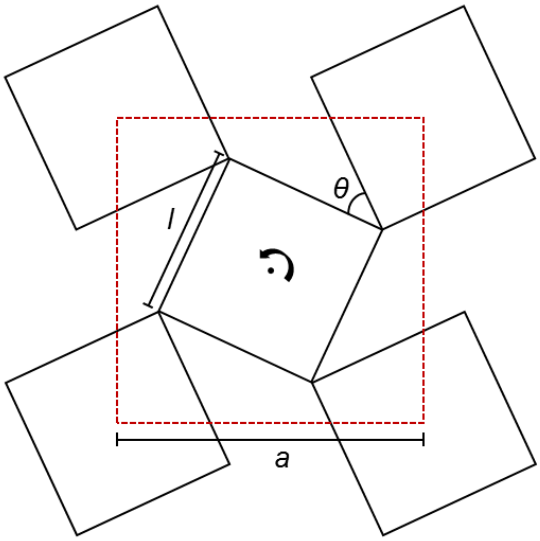

Fig. S10. Schematic representation in a corotating model. *a*: length of unit cell, *l*: width of cuboid (equal to d_1)

$$a^2 = 2l^2(1 + \sin\theta) \quad \text{(S2)}$$

$$l = 17.32 \text{ Å (average value)} \quad \text{(S3)}$$

The values of *l* are measured from crystal structure depending on temperature and 17.32 (average value) was obtained from average of measured value of *l*.

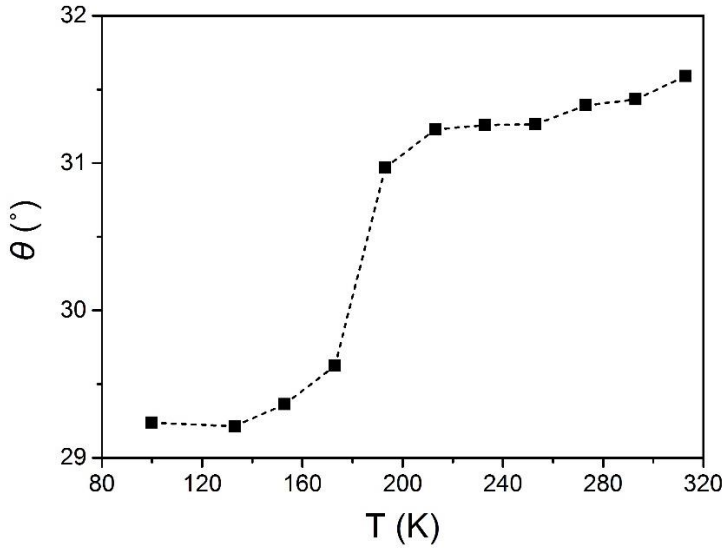

Fig. S11. Calculated θ values from temperature-dependent PXRD data of UPF-1.

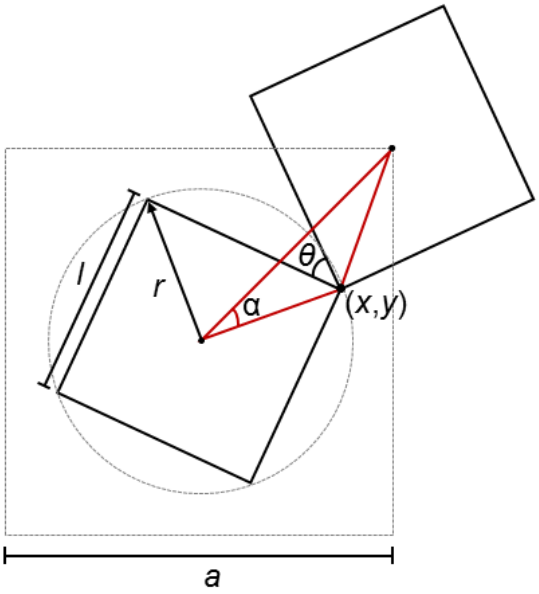

Fig. S12. Schematic illustration of the corotating model. α: angle of an isosceles triangle, *r*: the radius of a circle, θ and (*x*, *y*) coordinates.

Relationship between (*x*, *y*) coordinate and θ

$$2r\cos a = \frac{\sqrt{2}}{2}a \tag{S4}$$

$$^{*}a = l\sqrt{2(1+\sin\theta)}, \qquad r = \frac{\sqrt{2}}{2}l \tag{S5}$$

$$\therefore\ \cos\alpha = \sqrt{\frac{1+\sin\theta}{2}}, \qquad \sin\alpha = \sqrt{\frac{1-\sin\theta}{2}} \tag{S6}$$

$$(x, y) = \left(\frac{1}{2} + \frac{r}{a}\cos\left(\frac{\pi}{4} - \alpha\right), \quad \frac{1}{2} + \frac{r}{a}\sin\left(\frac{\pi}{4} - \alpha\right)\right) \tag{S7}$$

$$\therefore\ x = \frac{1}{4}\left(3 + \frac{\cos\theta}{1 + \sin\theta}\right), \quad y = \frac{1}{4}\left(3 - \frac{\cos\theta}{1 + \sin\theta}\right) \tag{S8}$$

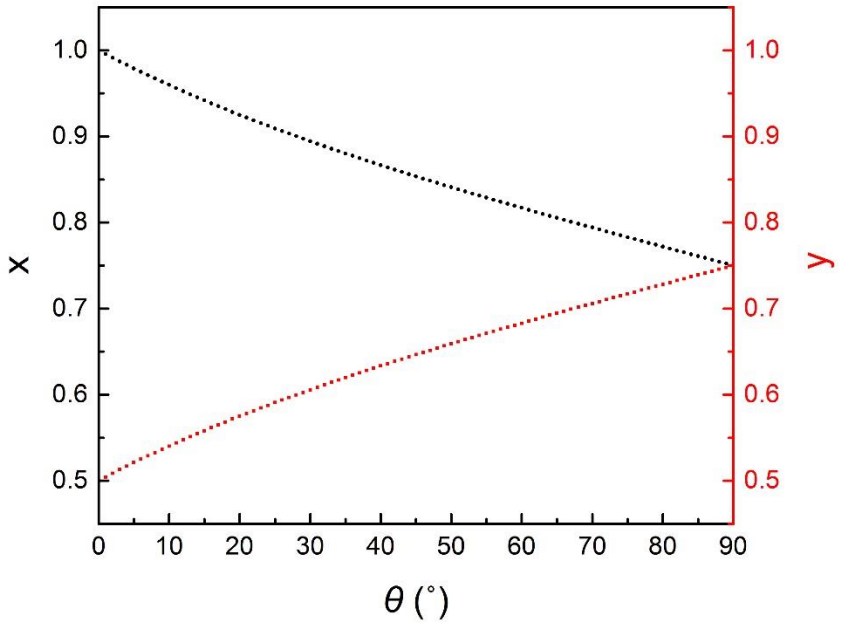

Fig. S13. Calculated (*x*, *y*) coordinates from 0° to 90°, derived from Equation.

Semi-empirical calculation of elastic constants

Elastic constants were calculated based on self-consistent charge density functional tight-binding (SCC-DFTB) method (*64*) with the third-order correction using 3OB-3-1 parameter set (*65, 66*) which is eligible to compute large-sized organometallic materials. From experimental X-ray crystal structures, the unit cell contains 1,196 atoms and its volume is 3.1 × 10^4 $Å^3$. We performed Γ-point calculation for the entire calculations.
The definition of Poisson's ratio (v_{ij}) is given by the negative ratio of the transverse strain (ϵ_{ii}) to the corresponding axial strain in a body subject to uniaxial stress (σ_{ii}) as

$$v_{ij} = -\frac{d\epsilon_{jj}}{d\epsilon_{ii}} = -\frac{d\, L_j/L_j^0}{d\, L_i/L_i^0} = -\frac{d \ln L_j}{d \ln L_i} \quad \text{(S9)}$$

where L_i is the strained lattice parameter. Especially Poisson's ratio on *xy*-plane is $v_{xy} = -\,d \ln L_y / d \ln L_x$.

We apply a uniaxial strain along the *x*-direction (ϵ_{xx}) and calculate the optimized L_y which is denoted as L_y^*. For this calculation, we assume that L_z (=*c* parameter) is constant since experimental results show that the change in L_z is only 0.24 % which is much smaller than the change in L_x (=*a* parameter) or L_y (=*b* parameter) which is 1.43 % as we increase a temperature from 193 K to 293 K. First, we obtain the optimized lattice parameters as well as the atomic positions, and the optimized lattice parameters are $L_x^0 = 29.874$ Å, $L_y^0 = 29.874$ Å, and $L_z^0 = 34.378$ Å while the experimental data gives $L_x^0 = 29.915$ Å, $L_y^0 = 29.915$ Å, and $L_z^0 = 34.378$ Å (at 193 K) which are in good agreement with each other.

We actually calculate v_{xy} from Eq. S10 by numerical differentiations as

$$v_{xy} = -\frac{d \ln L_y}{d \ln L_x} = -\frac{\epsilon_{yy}^{\alpha+1} - \epsilon_{yy}^{\alpha-1}}{2\Delta\epsilon_{xx}} \quad \text{(S10)}$$

where $\Delta\epsilon_{xx}$ = 0.026 %. For a given strain ϵ_{xx}^{α}, i.e. each L_x, we apply additional strains $\Delta\epsilon_{xx}$ (forward and backward) and obtain L_y^* to calculate $\epsilon_{yy}^{\alpha\pm1}$.

Table S7. Optimized lattice parameters L_y (L_y^*) and bond angles Zn─O─Zn projected on the *xy* plane with respect to strained L_x's.

L_x (Å)	L_y^* (Å)	L_y^*/L_x	Zn−O−Zn (°)
29.835	29.840	1.000	115.76
29.915	29.918	1.000	116.25
30.026	30.026	1.000	116.95
30.135	30.136	1.000	117.50
30.275	30.274	1.000	118.38
30.412	30.411	1.000	118.43

Various elastic constants are calculated from constitutive equations (*67*−*69*). Using Voigt notation, the relation between strains ϵ_i and stresses σ_i can be written as

$$\sigma_i = \sum_{j=1}^{6} C_{ij}\epsilon_j \tag{S11}$$

where C_{ij} is stiffness tensor of material properties. For tetragonal materials, we have six independent elastic constants: C_{11}, C_{12}, C_{13}, C_{33}, C_{44}, and C_{66}. To determine these elements, we apply six independent deformations, D_i (i = 1, · · ·, 6), to lattice vectors such as

$$D_1 = \begin{pmatrix} 1+\delta & 0 & 0 \\ 0 & 1+\delta & 0 \\ 0 & 0 & 1 \end{pmatrix} \tag{S12}$$

$$D_2 = \begin{pmatrix} 1+\delta & 0 & 0 \\ 0 & 1+\delta & 0 \\ 0 & 0 & \dfrac{1}{(1+\delta)^2} \end{pmatrix} \tag{S13}$$

$$D_3 = \begin{pmatrix} 1 & 0 & 0 \\ 0 & 1 & 0 \\ 0 & 0 & 1+\delta \end{pmatrix} \tag{S14}$$

$$D_4 = \begin{pmatrix} \left(\dfrac{1+\delta}{1-\delta}\right)^{\frac{1}{2}} & 0 & 0 \\ 0 & \left(\dfrac{1-\delta}{1+\delta}\right)^{\frac{1}{2}} & 0 \\ 0 & 0 & 1 \end{pmatrix} \tag{S15}$$

$$D_5 = \begin{pmatrix} 1 & 0 & \delta \\ 0 & 1 & \delta \\ \delta & \delta & 1+\delta^2 \end{pmatrix} \tag{S16}$$

and

$$D_6 = \begin{pmatrix} (1+\delta^2)^{\frac{1}{2}} & \delta & 0 \\ \delta & (1+\delta^2)^{\frac{1}{2}} & 0 \\ 0 & 0 & 1 \end{pmatrix} \tag{S17}$$

From the above deformations D_i, we can obtain following equations

$$E = E_0 + V_0\big((C_{11} + C_{12})\delta^2 + O(\delta^3)\big) \tag{S18}$$

$$E = E_0 + V_0\left((C_{11} + C_{12} + 2C_{33} - 4C_{13})\delta^2 + O(\delta^3)\right) \quad \text{(S19)}$$

$$E = E_0 + V_0\left(\frac{C_{33}}{2}\delta^2 + O(\delta^3)\right) \quad \text{(S20)}$$

$$E = E_0 + V_0\left((C_{11} - C_{12})\delta^2 + O(\delta^3)\right) \quad \text{(S21)}$$

$$E = E_0 + V_0\left(4(C_{44})\delta^2 + O(\delta^3)\right) \quad \text{(S22)}$$

and

$$E = E_0 + V_0\left(2(C_{66})\delta^2 + O(\delta^3)\right) \quad \text{(S23)}$$

respectively.

Thus, with a small δ, we can obtain C_{ij}'s based on quadratic fittings. Energies were calculated as a function of δ for D_i's. Quadratic functions are well fitted to the data points.

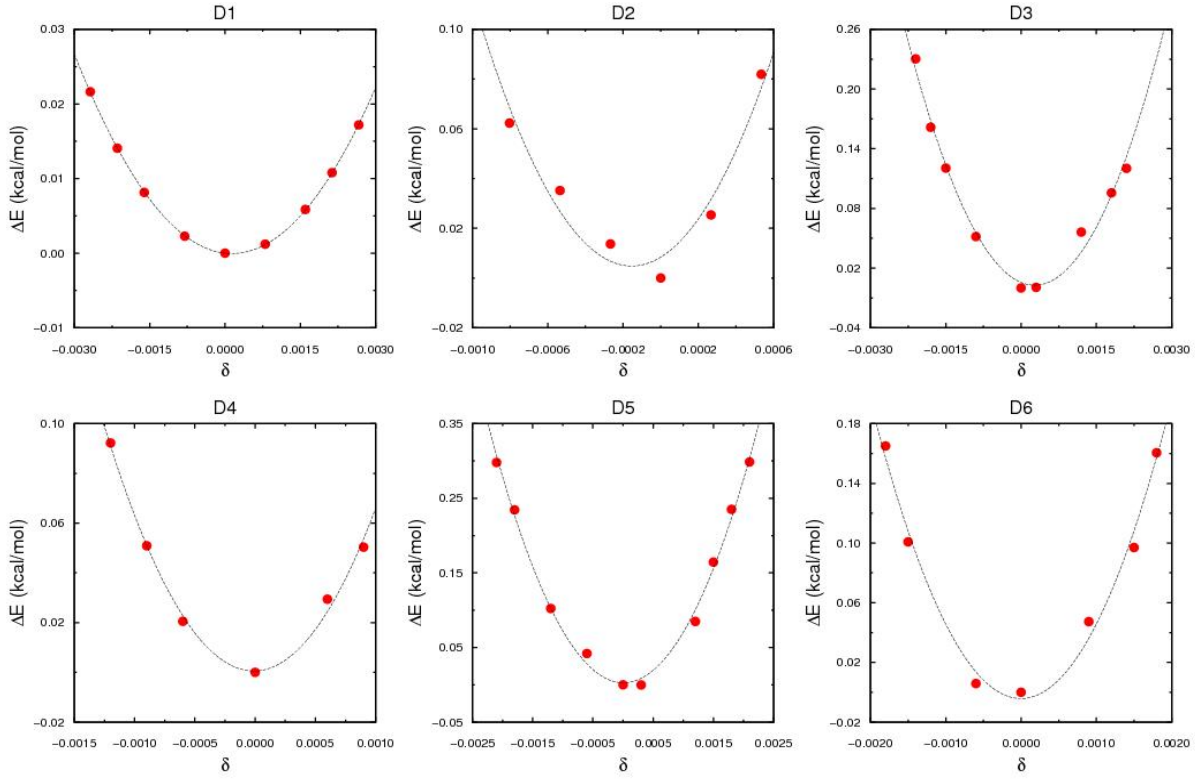

Fig. S14. Energy as a function of deformations D_i's. The dotted lines are quadratic functions from least-square fitting procedure.

We can obtain Young's modulus (E), Poisson's ratio (v), shear modulus (G), and bulk modulus (B) in terms of C_{ij}'s as

$$\begin{pmatrix} \epsilon_1 \\ \epsilon_2 \\ \epsilon_3 \\ \epsilon_4 \\ \epsilon_5 \\ \epsilon_6 \end{pmatrix} = \begin{pmatrix} \frac{1}{E_1} & -\frac{v_{12}}{E_1} & -\frac{v_{13}}{E_2} & 0 & 0 & 0 \\ -\frac{v_{12}}{E_1} & \frac{1}{E_1} & -\frac{v_{13}}{E_2} & 0 & 0 & 0 \\ -\frac{v_{13}}{E_2} & -\frac{v_{13}}{E_2} & -\frac{1}{E_2} & 0 & 0 & 0 \\ 0 & 0 & 0 & \frac{1}{2G_1} & 0 & 0 \\ 0 & 0 & 0 & 0 & \frac{1}{2G_1} & 0 \\ 0 & 0 & 0 & 0 & 0 & \frac{1}{2G_2} \end{pmatrix} \begin{pmatrix} \sigma_1 \\ \sigma_2 \\ \sigma_3 \\ \sigma_4 \\ \sigma_5 \\ \sigma_6 \end{pmatrix} \quad \text{(S24)}$$

For the calculation of bulk modulus, we have two representations; Voigt and Reuss methods as

$$B_V = \frac{1}{9}[2(C_{11} + C_{12}) + 4C_{13} + C_{33}] \quad \text{(S25)}$$

and

$$B_R = \frac{(C_{11} + C_{12})C_{33} - 2C_{13}^2}{C_{11} + C_{12} + 2C_{33} - 4C_{13}} \quad \text{(S26)}$$

The bulk modulus (B) for anisotropic materials is calculated from two methods such as Voigt (B_V) and Reuss (B_R). Average of the two values is used for anisotropic materials. The averaged bulk modulus $\left(B = 1/2\,(B_V + B_R)\right)$ is 1.268 GPa. Young's moduli of UPF-1 are high anisotropic. The lower value corresponds to the direction involving the change of the

Zn−O−Zn angle without the compression of bond length, while the higher value corresponds to the compression of bond length. The bulk modulus is usually related to the flexibility or stability of the materials. In general, the small bulk modulus means a flexible, but less stable structure. These stabilities can be checked from the necessary and sufficient elastic conditions (*69*). For tetragonal geometry, there are four following conditions $C_{11} > |C_{12}|, (C_{11} + C_{12})C_{33} < 2C_{13}^2, C_{44} > 0,$ and $C_{66} > 0$. UPF-1 shows comparable values for C_{11} and $|C_{12}|$, which can be interpreted as UPF-1 exists near stability boundary. Therefore, the bulk modulus of UPF-1 is as small as polymers.

Table S8. Stiffness tensor components (C_{ij}'s) of UPF-1 in GPa. The tetragonal crystal symmetry involves 6 independent components.

C_{11}	C_{12}	C_{13}	C_{33}	C_{44}	C_{66}
7.552	−6.937	0.336	17.492	3.886	5.647

Table S9. Elastic constants of UPF-1. Young's (*E*), shear (*G*) and bulk (*B*) modulus in GPa and Poisson's ratio (*v*).

E_1	E_2	G_1	G_2	B_V	B_R	v_{12}	v_{13}
1.156	17.123	1.943	2.823	2.230	0.307	−0.920	0.547

Table S10. Poisson's ratio of a variety of materials.

Compound	ν_{min}	ν_{max}	Ref
UPF-1	−1 (ν_{xy})		This work
^{C98}RhuA crystals	−1.00 ± 0.01		*23*
pyrite (cubic single crystal)	−0.14		*19*
Al(001) nanoplate (25a_0)	−3.2	4.6	*21*
α-cristobalite	−0.5		*17*
single-layer black phosphorus (*y*-direction)	−0.027		*20*
graphene sponges	~ 0		*9*
polyurethane	−0.7		*11*
MIL-53 (Al) lp	−2.4	1.9	*70*
MIL-53 (Ga) lp	−6.2	2.9	
MIL-47	−1.5	2.2	
DMOF-1 loz	−0.4	3.2	
DMOF-1 sq	0	1	
MOF-5	0.03	0.67	
IRMOF-1	0.29		*71*
ZIF-8	0.33	0.57	*72*
MIL-122(In)	−0.2	0.7	*42*
MOF-C6	0.13	0.27	*39*
MOF-C10	0.12	0.17	
MOF-C16	0.14	0.19	
MOF-C22	0.11	0.16	
MOF-C30	0.05	0.13	
$[NH_4][Zn(HCOO)_3]$	0.07		*40*
ZIF-4	−0.11	0.47	*73*
ZIF-zni	0.2	0.67	
HKUST-1 (B3LYP)	−0.31	1.21	*43*
HKUST-1 (B3LYP-D)	−0.28	1.19	
ZIF-1	0.03	0.63	*74*
ZIF-2	0.07	0.56	
ZIF-3	−0.43	1.34	
ZIF-4	0.06	0.41	
MIL-140A	−0.13	1.11	*44*
MIL-140B	−0.15	0.98	
MIL-140C	−0.29	1.16	
MIL-140D	−0.61	1.37	
$Zn[Au(CN)_2]_2$	0.02	1.1	*75*
ZIF-zni	0.32	0.49	*76*